Optics Letters

Broadband chaos of an interband cascade laser with a 6-GHz bandwidth

Yi-Bo Peng,[1,2,3,†] Zhecheng Dai,[1,2,3,†] Kai-Li Lin,[1] Peng-Lei Wang,[1,2,3] Zhijian Shen,[1,2,3] Baile Chen,[1,4] Frédéric Grillot,[5] and Cheng Wang[1,4,*]

[1]School of Information Science and Technology, ShanghaiTech University, Shanghai 201210, China
[2]Shanghai Institute of Microsystem and Information Technology, Chinese Academy of Sciences, Shanghai 200050, China
[3]University of Chinese Academy of Sciences, Beijing 100049, China
[4]Shanghai Engineering Research Center of Energy Efficient and Custom AI IC, ShanghaiTech University, Shanghai 201210, China
[5]LTCI, Télécom Paris, Institut Polytechnique de Paris, Palaiseau 91120, France
[†]These authors contribute equally to this work.
[*]wangcheng1@shanghaitech.edu.cn

Received 3 April 2024; revised 11 May 2024; accepted 14 May 2024; posted 15 May 2024; published 29 May 2024

Near-infrared semiconductor lasers subject to optical feedback usually produce chaos with a broad bandwidth of a few GHz. However, the reported mid-infrared interband cascade lasers (ICLs) only show chaos with a limited bandwidth below 1 GHz. Here we show that an ICL with optical feedback is able to generate broadband chaos as well. The mid-infrared chaos exhibits a remarkable bandwidth of about 6 GHz, which is comparable to that of the near-infrared counterpart. In addition, the spectral coverage in the electrical domain reaches as high as 17.7 GHz. It is found that the chaos bandwidth generally broadens with increasing feedback ratio and/or increasing pump current of the laser, while it is insensitive to the feedback length.

https://doi.org/10.1364/OL.525636

Near-infrared semiconductor lasers subject to proper external perturbation usually produce broadband chaos [1]. Commonly employed perturbation techniques include optical feedback, optical injection, and optoelectronic feedback [2]. Among these, optical feedback is the most popular method, because it simply requires an external mirror to provide the light reflection in the experimental configuration. The chaos bandwidth of near-infrared semiconductor lasers usually ranges from a few GHz up to tens of GHz (about 40 GHz), which is primarily governed by the relaxation oscillation (RO) frequency of lasers [3]. Taking advantage of the broad chaos bandwidth, near-infrared laser chaos has enabled high-speed secure optical fiber communications [4]. The maximum data transmission rate is roughly limited by the chaos bandwidth, and the reported transmission rate reaches up to 100 Gbps [5]. In addition, the irregular nature of chaos has been employed for the random number generation with an ultra-fast speed [6]. The bit generation speed is limited by the chaos bandwidth as well, and the reported generation rate reaches as high as a few Tbps [7,8]. Interestingly, the laser chaos is also useful for developing lidar systems, where the time of flight is extracted from the cross correlation of the local chaos waveform and the target-reflected chaos waveform [9]. The ranging distance of chaotic lidars reaches more than 100 m with a sub-centimeter precision associated with a sub-centimeter accuracy [10]. On the other hand, the ranging resolution of chaotic lidars is also determined by the bandwidth of chaos [11]. Consequently, raising the bandwidth of chaotic laser sources is vital for improving the performance of the above three applications.

Owing to the low-loss transmission windows of the atmosphere in the wavelength ranges of 3–5 and 8–12 μm, the mid-infrared laser chaos holds great potential for developing remote free-space secure communication links and long-reach chaotic lidar systems [12]. One method for the generation of mid-infrared chaos is based on quantum cascade lasers (QCLs). However, the measured chaos bandwidth of QCLs is only a few MHz so far [13,14], which is much smaller than the intrinsic modulation bandwidth of QCLs [15]. This is because the carrier lifetime of QCLs is smaller than the photon lifetime, and hence the nonlinear dynamics resemble that of class-A lasers [16]. On the other hand, the simulation in [17] showed that QCLs can produce broadband chaos as well. Private communication based on the chaos of QCLs has been successfully demonstrated with a transmission rate of 0.5 Mbit/s [18]. Recent work showed the data encryption with the chaos of QCLs in the long wavelength infrared atmospheric window, and the transmission rate reached 8 Mbit/s [19]. Another method for generating mid-infrared chaos relies on interband cascade lasers (ICLs). In contrast to QCLs, the laser emission of ICLs is based on the interband transition of carriers within type-II quantum wells [20]. Most GaSb-based ICLs work in the wavelength range of 3–6 μm, while InAs-based ICLs extend the wavelength up to more than 10 μm [21]. The carrier lifetime of ICLs is on the order of sub-nanosecond, and thereby ICLs are typical class-B lasers. The development of high-speed ICLs is much less mature than common near-infrared lasers, and the reported modulation bandwidths of ICLs range from a few hundreds of MHz up to 5 GHz [22,23]. Our previous work demonstrated that an ICL with optical feedback produced chaos with a bandwidth of 465 MHz, and the spectral coverage in the electrical domain reaches over 2 GHz [24]. Zhao *et al.* also observed that the chaos bandwidth of an ICL was less than 400 MHz [25]. Moreover, Grillot *et al.* reported that the

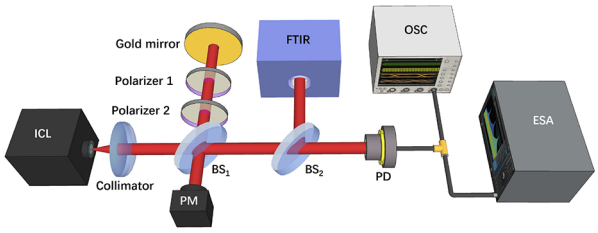

Fig. 1. Experimental setup for the mid-infrared chaos generation. BS, beam splitter; FTIR, Fourier transform infrared spectrometer, PM: power meter; PD, photodetector; ESA, electrical spectrum analyzer; OSC, oscilloscope.

chaos bandwidth of an ICL with optical feedback could reach about 1 GHz [26]. In addition to the perturbation of the optical feedback, our recent work showed that an ICL subject to optical injection produced chaos as well, and the chaos bandwidth is about 320 MHz [27]. The nonlinear dynamics of an ICL with optoelectronic feedback have been also investigated, but chaos was not observed [28]. In this work, we experimentally demonstrate that an ICL with optical feedback produces a broadband chaos with a record value of 5.9 GHz. This chaos bandwidth is comparable to that of near-infrared semiconductor lasers. In addition, the spectral coverage of the chaos signal in the electrical domain reaches as broad as 17.7 GHz.

Figure 1 illustrates the experimental setup for the generation of the mid-infrared chaos using an ICL subject to optical feedback. The ICL under study is a commercial single-mode distributed feedback laser (Nanoplus), with a cavity length of 900 μm and a ridge width of 3 μm. The front facet is anti-reflection coated, and the rear facet is high-reflection coated. The ICL is pumped by a DC current source, and the operation temperature is maintained at 20°C by a thermoelectric cooler. The optical feedback is provided by a gold mirror, which is located 50 cm away from the ICL device (unless stated otherwise). The feedback strength is adjusted by the combination of two polarizers, where polarizer 2 is aligned to the TE polarization of the ICL, and polarizer 1 is rotated to vary the feedback strength. The feedback ratio is defined as the ratio of the reflected power by the mirror to the laser output power. The feedback light power is monitored by a power meter (PM). The optical spectrum is measured by a Fourier transform infrared spectrometer (FTIR) with a resolution of 0.08/cm. The electrical spectrum is measured by a broadband electrical spectrum analyzer (ESA) with a bandwidth of 50 GHz, and the resolution bandwidth is fixed at 3 MHz. The temporal waveform is recorded on a high-speed digital oscilloscope (OSC) with a bandwidth of 59 GHz, and the sampling rate is fixed at 80 GSample/s. In literature, the mid-infrared optical signal is converted to the electrical one mostly by a commercial HgCdTe photodetector (PD). However, the detection bandwidth of HgCdTe PD is usually less than 1 GHz, which is likely to limit the detection of the broadband chaos. In order to circumvent the bandwidth limitation, we employ a homemade uni-traveling carrier (UTC) PD with a detection bandwidth of 12.8 GHz and the responsivity is 0.8 A/W at room temperature. The PD device was grown on a GaSb substrate using molecular beam epitaxy. The active region started with a 300 nm thick InAs/AlAsSb superlattice (SL) bottom contact layer followed by 50 nm thick n-type InAsSb. The drift layer is 420 nm thick unintentionally doped InAsSb, followed by a 900 nm InAs/InAsSb SL absorption layer with four-step graded p-type doping. After that, 50 nm

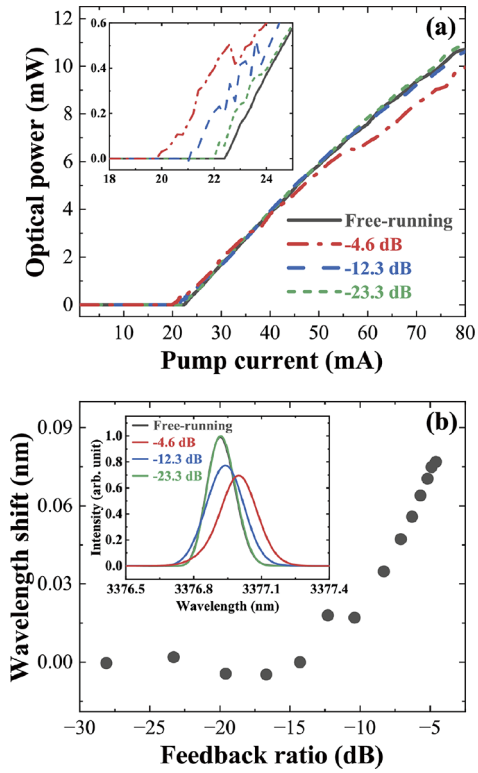

Fig. 2. (a) L–I curves of the ICL with optical feedback. Inset shows the zoom-in L–I curves near the lasing threshold. (b) Wavelength shift as a function of the feedback ratio at $1.3 \times I_{th}$. Inset shows the optical spectra for several feedback ratios.

thick AlAsSb/AlSb SL was added as a barrier layer. The top is a 10 nm thick InAsSb contact layer. For more details about the UTC PD refer to [29,30].

As shown in Fig. 2(a), the free-running ICL exhibits a lasing threshold of $I_{th} = 22.4$ mA, and the laser power saturates around 11 mW. When applying the optical feedback to the ICL, the lasing threshold of the ICL decreases [inset of Fig. 2(a)], and it goes down to 20.0 mA at the feedback ratio of $R = -4.6$ dB. For pump currents slightly above the lasing threshold, the optical feedback raises the optical power. However, for pump currents above 36.0 mA, the optical power either increases or decreases depending on the feedback phase [31]. The inset of Fig. 2(b) shows that the free-running ICL emits a single mode around 3376.9 nm when it is pumped at $1.3 \times I_{th}$. For feedback ratios below −14 dB, the lasing wavelength in Fig. 2(b) has little variation. However, stronger feedback strength redshifts the lasing wavelength nonlinearly by more than 0.07 nm. This is due to the fact that the optical feedback reduces the gain of the laser medium, which in turn raises the refractive index [31].

Figures 3(a) and 3(b) show the evolution of the nonlinear dynamics of the ICL with optical feedback at $1.3 \times I_{th}$. When the feedback strength is weak, such as $R = -23.3$ dB in Fig. 3(a), the ICL remains to produce a continuous wave, which is similar to the free-running case. When increasing the feedback strength to $R = -12.3$ dB, the ICL starts to produce quasi-periodic oscillations. The corresponding electrical spectrum in Fig. 3(b) exhibits multiple peaks, and the peak interval is 287 MHz. The appearance of the peaks is due to the external cavity modes of the optical feedback, and the peak interval is determined by the inverse of the round trip feedback delay time (3.5 ns). At the feedback ratio

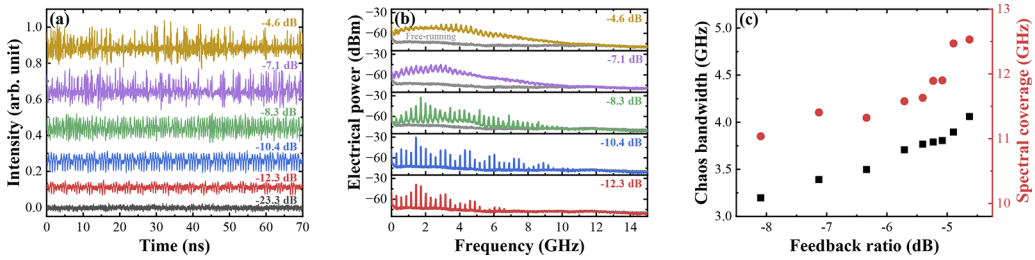

Fig. 3. Evolution of the ICL dynamics toward chaos (a) in the temporal domain and (b) in the electrical domain. (c) Chaos bandwidth (squares) and spectral coverage (dots) as a function of the feedback ratio. The pump current is $1.3 \times I_{th}$.

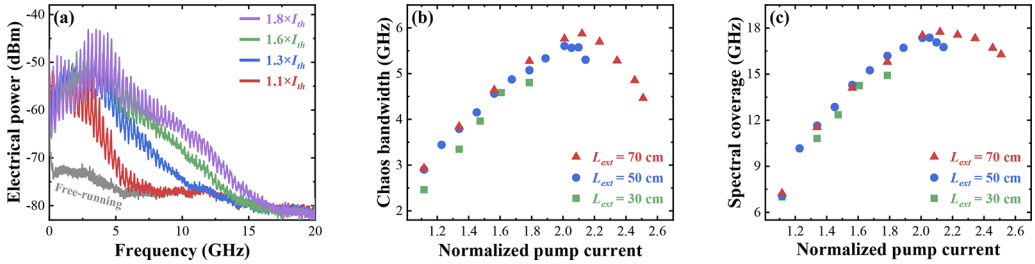

Fig. 4. (a) Electrical spectra of chaos at several pump currents. The feedback length is 50 cm. (b) Chaos bandwidth and (c) spectral coverage versus the normalized pump current at different feedback lengths. The feedback lengths in (b) and (c) are 30 cm (squares), 50 cm (dots), and 70 cm (triangles), respectively. The feedback ratio is fixed at $R = -4.6$ dB.

of $R = -10.4$ dB, the ICL still produces quasi-periodic oscillations, but with a higher oscillation speed and a larger oscillation amplitude in Fig. 3(a). Correspondingly, the electrical spectrum in Fig. 3(b) shows more external cavity modes. When the feedback strength is increased to $R = -8.3$ dB, the time trace in Fig. 3(a) becomes irregular, which suggests the onset of chaos. This chaos onset is about 20 dB higher than that of common near-infrared lasers. Indeed, the background power level of the electrical spectrum in Fig. 3(b) becomes higher than that of the free-running case. However, the chaotic oscillations still involve strong periodic components in the electrical spectrum. Further increasing the feedback strength enhances the randomness of the chaotic waveform. The temporal waveforms at $R = -7.1$ dB and $R = -4.6$ dB in Fig. 3(a) become more and more irregular, and hence the corresponding chaos are more complex. The corresponding electrical spectrum in Fig. 3(b) gradually rises and broadens. At the feedback ratio of $R = -4.6$ dB, the electrical power is more than 10 dB higher than the background noise level for Fourier frequencies below 4.0 GHz. Meanwhile, the signature of external cavity modes becomes much weaker in comparison with the chaos at the onset of $R = -8.3$ dB. The evolution of the nonlinear dynamics proves that the ICL follows the quasi-periodic route to chaos, which is the typical route for common near-infrared semiconductor lasers with optical feedback [32]. Figure 3(c) shows the chaos bandwidth and the spectral coverage based on the analysis of the electrical spectrum. The chaos bandwidth is defined as the frequency span between the DC and the cutoff frequency, which contains 80% of the total power in the electrical spectrum [33]. The spectral coverage is defined as the frequency span where the power is higher than the free-running case. It is shown that both the chaos bandwidth and the spectral coverage rise nonlinearly with the increasing feedback strength, which are similar to the case of common near-infrared lasers [34]. The chaos bandwidth increases from 3.2 GHz at $R = -8.1$ dB to 4.1 GHz at $R = -4.6$ dB. Meanwhile, the spectral coverage increases from 11.0 to 12.5 GHz. Both the enhanced chaos bandwidth and the spectral coverage are attributed to the nonlinear interaction between the RO frequency and the external cavity frequency as the feedback strength increases [1].

Figure 4 depicts the effect of the pump current on the chaos dynamics, where the feedback ratio is fixed at $R = -4.6$ dB. It is found that the ICL produces broadband chaos for a wide range of pump currents, from the near-threshold condition to the well above-threshold condition. Figure 4(a) demonstrates that the electrical spectrum of the chaos broadens with increasing pump current. In addition, the peak frequency of the electrical spectrum generally increases from 2.3 GHz at $I = 1.1 \times I_{th}$ up to 3.8 GHz at $I = 1.8 \times I_{th}$. This is because the RO frequency of semiconductor lasers rises with the pump current, and the RO frequency roughly determines the peak frequency of the chaos spectrum [35]. Judging from the envelope peak of the chaos spectrum, the RO frequency f_{RO} of the ICL is estimated to be in the range of 2 to 5 GHz, which is an order of magnitude larger than the external cavity frequency ($f_{ext} = 287$ MHz). This means the optical feedback in the experiment is operated in the long external cavity regime ($f_{RO} >> f_{ext}$). The chaos bandwidth in Fig. 4(b) first rises with the pump current to a maximum value and then declines, which is similar to the evolution trend of near-infrared lasers [36]. For the feedback length of $L_{ext} = 50$ cm (dots), the maximum chaos bandwidth is 5.6 GHz, which is achieved at the pump current of $I = 2.0 \times I_{th}$. For the feedback length of $L_{ext} = 70$ cm (triangles), the maximum chaos bandwidth slightly increases to 5.9 GHz, which is obtained at $I = 2.1 \times I_{th}$. Further increasing the pump current reduces the chaos bandwidth, which can be attributed to the increased damping factor [35]. The behavior of the chaos bandwidth is similar to the modulation bandwidth of semiconductor lasers, which reaches the maximum at an optimal pump current. However, for the feedback length of $L_{ext} = 30$ cm (squares), the chaos bandwidth always increases with the pump current from 2.5 GHz at $I = 1.1 \times I_{th}$ up to 4.8 GHz at $I = 1.8 \times I_{th}$. The chaos does not occur anymore

for pump currents above $1.8 \times I_{th}$. On one hand, this is because semiconductor lasers are less sensitive to optical feedback with a shorter feedback length [37,38]. On the other hand, the large damping factor at a high pump current raises the onset feedback ratio of the chaos. Consequently, the chaos occurs in a broader operation range of pump currents for the ICL with a longer feedback length in Fig. 4(b). For pump currents below $1.8 \times I_{th}$, however, the feedback length has little impact on the chaos bandwidth. This is different from the case of the short external cavity regime ($f_{RO} << f_{ext}$), where a shorter feedback length leads to a broader chaos bandwidth owing to the enhanced RO frequency [39]. The evolution trend of the spectral coverage in Fig. 4(c) is similar to that of the chaos bandwidth in Fig. 4(b). The maximum spectral coverage is as broad as 17.7 GHz, which is realized at the feedback length of $L_{ext} = 70$ cm, associated with the pump current of $I = 2.1 \times I_{th}$. Both the above chaos bandwidth and the spectral coverage of the ICL chaos are comparable to those of common near-infrared lasers.

It is remarked that the chaos bandwidth of ICLs can be enhanced by raising the RO frequency, through the optimization of the cascading gain stages and/or the laser cavity parameters [40]. However, the chaos bandwidth is likely to be affected by the large damping factor of ICLs, which arises from the strong gain compression effect [22]. A comprehensive understanding of the physical mechanisms governing the RO frequency of ICLs remains required in future work. On the other hand, the chaos bandwidth can be further raised by applying proper external perturbations, such as optical injection, mutual injection, phase-conjugate optical feedback, and filtered optical feedback [41]. It is expected that the chaos bandwidth of ICLs can reach more than 10 GHz or even tens of GHz, through the above two optimization methods.

In summary, we have experimentally demonstrated that an ICL with the perturbation of optical feedback is able to produce broadband chaos in the mid-infrared regime. The chaos bandwidth reaches the record value of about 6 GHz, and the spectral coverage in the electrical domain is as large as 17.7 GHz. Generally, raising the feedback ratio and/or raising the pump current broadens the chaos bandwidth and the spectral coverage. However, the feedback length has little impact on the chaos bandwidth. This broadband mid-infrared chaotic laser source is helpful for developing remote free-space secure communication links with a high transmission capacity, and for constructing long-reach chaotic lidar systems with a high resolution.

Funding. Natural Science Foundation of Shanghai (20ZR1436500).

Acknowledgment. The authors acknowledge the fabrication support from the Quantum Device Lab of ShanghaiTech University.

Disclosures. The authors declare no conflicts of interest.

Data availability. Data underlying the results presented in this paper are not publicly available at this time but may be obtained from the authors upon reasonable request.

REFERENCES

1. A. Uchida, *Optical Communication with Chaotic Lasers* (Wiley, 2012).
2. M. Sciamanna and K. A. Shore, Nat. Photonics **9**, 151 (2015).
3. L. Qiao, T. Lv, Y. Xu, *et al.*, Opt. Lett. **44**, 5394 (2019).
4. A. Argyris, D. Syvridis, L. Larger, *et al.*, Nature **438**, 343 (2005).
5. Y. Xie, Z. Yang, M. Shi, *et al.*, Adv. Photonics Nexus **3**, 016003 (2023).
6. J.-C. Li, J.-L. Xiao, Y.-D. Yang, *et al.*, Nanophotonics **12**, 4109 (2023).
7. B. Shen, H. Shu, W. Xie, *et al.*, Nat. Commun. **14**, 4590 (2023).
8. P. Li, Q. Li, W. Tang, *et al.*, Light: Sci. Appl. **13**, 66 (2024).
9. R. Chen, H. Shu, B. Shen, *et al.*, Nat. Photonics **17**, 306 (2023).
10. C.-H. Cheng, C.-Y. Chen, J.-D. Chen, *et al.*, Opt. Express **26**, 12230 (2018).
11. A. Lukashchuk, J. Riemensberger, A. Tusnin, *et al.*, Nat. Photonics **17**, 814 (2023).
12. H. Lin, L. Li, Y. Zou, *et al.*, Proc. SPIE **8600**, 86000K (2013).
13. L. Jumpertz, K. Schires, M. Carras, *et al.*, Light: Sci. Appl. **5**, e16088 (2016).
14. O. Spitz, J. Wu, A. Herdt, *et al.*, IEEE J. Sel. Top. Quantum Electron. **25**, 1200311 (2019).
15. R. Paiella, R. Martini, F. Capasso, *et al.*, Appl. Phys. Lett. **79**, 2526 (2001).
16. J. Ohtsubo, *Semiconductor Lasers: Stability, Instability and Chaos* (Springer, 2017).
17. C. Chen, Z. Jia, Y. Lv, *et al.*, Opt. Lett. **46**, 5039 (2021).
18. O. Spitz, A. Herdt, J. Wu, *et al.*, Nat. Commun. **12**, 3327 (2021).
19. P. Didier, S. Zaminga, O. Spitz, *et al.*, Optica **11**, 626 (2024).
20. C.-H. Lin, R. Q. Yang, D. Zhang, *et al.*, Electron. Lett. **33**, 598 (1997).
21. I. Vurgaftman, W. W. Bewley, C. L. Canedy, *et al.*, Nat. Commun. **2**, 585 (2011).
22. Z.-F. Fan, Y. Deng, C. Ning, *et al.*, Appl. Phys. Lett. **119**, 081101 (2021).
23. B. Schwarz, J. Hillbrand, M. Beiser, *et al.*, Optica **6**, 890 (2019).
24. Y. Deng, Z.-F. Fan, B.-B. Zhao, *et al.*, Light: Sci. Appl. **11**, 7 (2022).
25. M. Zhao, G. Xia, K. Yang, *et al.*, Photonics **9**, 410 (2022).
26. F. Grillot, O. Spitz, S. Zhao, *et al.*, Proc. SPIE **12430**, 1243005 (2023).
27. K.-L. Lin, P.-L. Wang, Y.-B. Peng, *et al.*, Opt. Express **32**, 16722 (2024).
28. J. Liu, Z. Wu, M. Zhao, *et al.*, Opt. Express **31**, 29012 (2023).
29. J. Huang, Z. Shen, Z. Wang, *et al.*, IEEE Electron Device Lett. **43**, 745 (2022).
30. J. Huang, Z. Dai, Z. Shen, *et al.*, IEEE Trans. Electron Devices **69**, 6890 (2022).
31. R. Lang and K. Kobayashi, IEEE J. Quantum Electron. **16**, 347 (1980).
32. J. Mørk, J. Mark, and B. Tromborg, Phys. Rev. Lett. **65**, 1999 (1990).
33. F. Y. Lin and J. M. Liu, Opt. Commun. **221**, 173 (2003).
34. E. Mercier, D. Wolfersberger, and M. Sciamanna, Sci. Rep. **6**, 18988 (2016).
35. L. A. Coldren, S. W. Corzine, and M. L. Masanovic, *Diode Lasers and Photonic Integrated Circuits* (Wiley, 2012).
36. J. P. Toomey, D. M. Kane, M. W. Lee, *et al.*, Opt. Express **18**, 16955 (2010).
37. J.-Y. Tang, B.-D. Lin, J. Yu, *et al.*, IEEE J. Quantum Electron. **58**, 8100109 (2022).
38. K. Petermann, IEEE J. Sel. Top. Quantum Electron. **1**, 480 (1995).
39. R. Takahashi, Y. Akizawa, A. Uchida, *et al.*, Opt. Express **22**, 11727 (2014).
40. Y. Deng and C. Wang, IEEE J. Quantum Electron. **56**, 2300109 (2020).
41. Q. Yang, L. Qiao, M. Zhang, *et al.*, Opt. Lett. **45**, 1750 (2020).